ORIGINAL RESEARCH PAPER

Fuel Cells DOI: 10.1002/fuce.201300026

Mechanical Properties of Gd-CeO_2 Electrolyte for SOFC Prepared by Aqueous Tape Casting

A. Akbari-Fakhrabadi[1]*, R. V. Mangalaraja[1]*, M. Jamshidijam[1], S. Ananthakumar[2], S. H. Chan[3]

[1] Advanced Ceramics and Nanotechnology Laboratory, Department of Materials Engineering, University of Concepcion, Concepcion, Chile

[2] Materials and Mineral Division, National Institute for Interdisciplinary Science and Technology, CSIR, Trivandrum-695019, Kerala, India

[3] School of Mechanical and Aerospace Engineering, Nanyang Technological University, Singapore

Received January 30, 2013; accepted April 19, 2013; published online June 10, 2013

Abstract

Mechanical properties of gadolinium-doped ceria ($Ce_{0.9}Gd_{0.1}O_{1.95}$, 10GDC) green tape prepared by aqueous-based tape casting process were characterized by tensile test and shear punch test (SPT). SPT was found to be a useful method for characterizing mechanical properties of green tapes. Microstructures and mechanical properties such as flexural modulus, bending strength, and microhardness of tapes sintered at 1,300–1,500 °C have been evaluated. Indentation fracture toughness was also determined by the method of Palmqvist cracks at different applied loads for tapes sintered at 1,500 °C. Grain size measurements showed that excessive grain growth occurred during sintering despite using 10GDC nanopowders as the starting material. However, mechanical properties of sintered tapes improved by increasing sintering temperature and the results are comparable with those reported for 10GDC in literature.

Keywords: Aqueous Tape Casting, Electrolyte, 10GDC, Mechanical Properties, Sintering, SOFC

1 Introduction

Solid oxide fuel cells (SOFCs) as an attractive candidate for the next power generation sources are one of the main topics in today's energy and the environment. Lowering of the operating temperature in order to reduce the hassle of balance of plant (BoP) and fabrication cost is a major technological challenge for their commercialization. Therefore, selecting high-ionic conducting electrolyte materials and developing low-cost and environmentally friendly fabrication techniques are the focus of recent studies [1, 2].

Gadolinium-doped ceria (GDC) solid solution formed by replacing the Ce^{4+} sites of the CeO_2 lattice by Gd^{3+} cations has been extensively studied as a promising candidate electrolyte material for intermediate and low temperature SOFCs [3]. Nevertheless, densification of GDC electrolyte requires high sintering temperatures above 1,500 °C for conventional sintering which results in large grain size and as a consequence mechanically unstable at the operating conditions [4]. Using nanosized 10GDC powder prepared by combustion synthesis, co-precipitation, sol–gel, and hydrothermal solution has been offered as a way to overcome this issue [5–12].

In the case of electrolyte-supported cells, the fabrication of the electrolyte is dominated by tape casting which is a well established and cost-effective method in the electroceramics industry and is scalable for mass production [13]. Tape casting often uses a slurry containing ceramic powder, solvent, binder, plasticizer, and additives such as de-foamer, surfactant, and dispersant [14]. Due to environmental, health, safety, and economic reasons, aqueous-based tape casting method using water as a solvent is adopted to replace the traditional organic-based tape casting method [15]. Despite these advantages, several critical challenges should be overcome which include slow drying rate of the tape, high crack sensitivity, low strength of water-soluble binders, and the agglomeration of powders due to hydrogen bonding [16–18]. Also, ceramic powder as main constituent of slurry plays an

[*] *Corresponding author, aliakbarif@udec.cl; mangal@udec.cl*

important role in suspension composition. Colloidally stable nanosized powder suspensions are known to have a markedly lower volume loading compared to suspensions with larger particle sizes [19]. As a consequence, the green bodies resulting from nanopowders usually have low green densities and are difficult to sinter to dense ceramics [20, 21].

The manageability of green bodies obtained by tape casting depends on the slurry formulation and can be evaluated by their mechanical properties such as flexibility, tensile, and shear strength. For example, tensile strength of zinc oxide [22], hydroxyapatite [14], SiC [23], $BaTiO_3$ [24], and alumina [18] green tapes has been reported. To-date, there is no information on mechanical properties of GDC green tapes.

When electrolyte is chosen as a support layer of SOFC especially for mobile applications, it must have sufficient mechanical properties to avoid cell failure due to damaged electrolyte. Despite many works have been studied the structural stability and electrical properties of GDC electrolyte, only a handful of reports dealt with its mechanical properties [25–28].

In this work, tensile test and shear punch test (SPT) have been applied to evaluate the mechanical properties of 10GDC green tape obtained by aqueous tape casting. Also, effect of sintering temperature on microstructure and mechanical properties such as bending modulus and strength, hardness, and fracture toughness of sintered tapes has been investigated.

2 Experimental

2.1 Aqueous Tape Casting 10GDC Electrolyte

$Ce_{0.9}Gd_{0.1}O_{1.95}$ (10GDC) nanopowders were synthesized by the nitrate-fuel combustion method. Citric acid was used as an organic fuel and high purity (>99.9%) cerium nitrate [$Ce(NO_3)_3{\cdot}6H_2O$] and gadolinium nitrate [$Gd(NO_3)_3{\cdot}6H_2O$] were used as precursor reagents. The details of the synthesis have been reported elsewhere [26, 29]. The slurry formula for aqueous tape casting 10GDC electrolyte substrate is summarized in Table 1. 10GDC powders were dispersed in distilled water with the pH adjusted within the range of 9–10 containing dispersant by ball milling. Then, the plasticizer, binder, defoamer, and surfactant were added to the slurry and ball milled to achieve good homogeneity. The laboratory-scale tape casting machine with single doctor blade and moving substrate was used. A casting speed of 100 mm min^{-1} and gap height of 1 mm were set. The suspensions were cast onto a silicone-coated mylar carrier film with a heating bed adjusted to 20 °C without blowing air and the tapes were left to dry naturally for 24 h. The green tape thicknesses were in the range of 300–400 μm. The details of the fabrication method have been reported elsewhere [1].

Table 1 The slurry formula of GDC aqueous tape casting.

Chemicals	Functions	wt.%
10GDC, $Ce_{0.9}Gd_{0.1}O_{1.95}$	Ceramic powder	45.6
Distilled water	Solvent	15
PVA, polyvinyl alcohol (70,000–100,000 g mol^{-1})	Binder[a)]	30
PEG, polyethylene glycol (200 g mol^{-1})	Plasticizer	8.3
PAA, polyacrylic acid (1,800 g mol^{-1})	Dispersant	0.8
2,4,7,9-Tetramethyl-5-decyne-4,7-diol ethoxylate	Surfactant	0.1
Octanol	Defoamer	0.2

[a)] The binder was prepared by dissolving PVA in distilled water (PVA/water ratio: 0.16).

2.2 Sintering

The samples were heated up to 600 °C at a rate of 30 °C h^{-1} and held for 1 h to slowly burn off all organic additives. They were then heated at 100 °C h^{-1} at sintering temperatures of 1,300, 1,400, and 1,500 °C for 2 h and cooled down at a cooling rate of 200 °C h^{-1}.

The diameter of the grains on surface of sintered tapes was measured by Image Analyzer. At least 300 grains were selected in each specimen to determine the average grain size and grain size distribution.

2.3 Mechanical Measurement of Green Tapes

The green tapes were kept for 24 h in humidity (63%) and temperature (24 °C) controlled room where tests were carried out using a Smar Tens 005 test machine with a load cell of 1 kN capacity. According to the ASTM standard D-638 V, six dog-bone tensile specimens were punched in parallel and transverse to the casting direction.

Disks of 12 mm in diameter were punched for the SPT. These specimens were placed in a shear punch fixture and deformed to failure against a receiving die of 3 mm diameter by a flat head punch of 2.95 mm diameter. The applied load as a function of punch displacement was obtained by a data logger in order to determine the shear stress of the tested materials by following relationship

$$\tau = \frac{P}{\pi d t} \tag{1}$$

where P is the punch load, d the average of the punch and die diameters, and t is the specimen thickness.

2.4 Mechanical Measurement of Sintered Tapes

The three point flexural strength and modulus of the sintered tapes was measured on the same machine used for tensile test and SPT using following equations:

$$\sigma_{\text{flex}} = \frac{3lP}{2wt^2} \tag{2}$$

$$E_{\text{flex}} = \frac{l^3 m}{4wt^3} \tag{3}$$

where P is the applied load, l the span width, w the width and t the thickness of the specimen, and m is the slope of the tangent to the initial straight-line portion of the load-deflection curve. The dimensions of the analyzed specimens were prepared as 35 × 4 × 0.2 mm^3 in parallel and transverse to

the casting direction. The bending tests were performed six times for each direction with a crosshead speed of 0.5 mm per min and a span width of 30 mm at room temperature.

The Vickers microhardness of the sintered tapes was measured using Struers microhardness tester under ambient conditions. The hardness was determined by the ratio of the applied load via a geometrically defined indenter to the projected area of the resultant impression using the relationship:

$$H_v = \frac{1,854.4P}{a^2} \quad (4)$$

where P is the applied load and a is the indentation diagonal length. In a typical indentation test, load was varied from 0.25 to 5 N for a dwelling time of 5 s. At least eight indentations were made for each load on all the samples.

The fracture toughness was determined by the indentation technique using the same instrument. Both diagonal lengths of the indentation images and crack lengths were measured by scanning electron microscopy (SEM, JEOL 6460 LV) and the fracture toughness (K_{IC}) values were calculated by the method of Palmqvist cracks using the equations proposed by Niihara et al. [30].

$$K_{IC} = 0.0089\left(\frac{E}{0.927H_v}\right)^{2/5}\frac{P}{a\sqrt{l}} \quad (5)$$

and Anstis et al. [31]:

$$K_{IC} = 0.016\left(\frac{E}{H_v}\right)^{1/2}\frac{P}{c^{3/2}} \quad c = a + l \quad (6)$$

where P is the applied load, H_v the Vickers hardness, E the elastic modulus of the material measured by bending test, and a and c are diagonal and crack length generated by the indentation.

3 Results and Discussion

3.1 Mechanical Properties of Green Tapes

As shown in Figure 1, the dried green tape was judged to be flexible according to Greenwood et al. [32] and easy to handle without being sensitive to mechanical stresses.

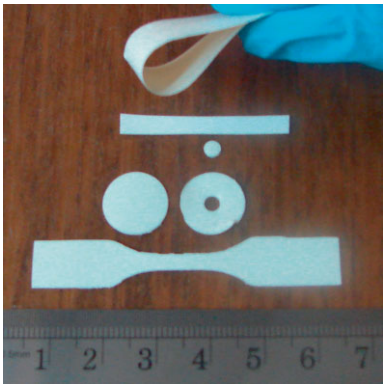

Fig. 1 Photograph of green tape showing its flexibility, along with samples for tensile, SPT, and flexural tests.

A typical stress–strain curve and fracture surface of green tape is demonstrated in Figure 2. As it can be seen, fracture occurred normal to the stress axis without noticeable plastic deformation and non-linear stress–strain curve resembles a quasi-brittle fracture. The tensile strength and elongation values obtained from tensile tests in parallel and transverse casting directions with different strain rates are listed in Table 2. These data do not show any anisotropy related to casting direction and are not significantly influenced by strain rate.

The tension test is widely used to provide basic information like tensile strength and elongation on the mechanical behavior of materials and as an acceptance test for the specification of materials. It is also used to measure strain rate sensitivity of these quantities [33]. However, tensile tests usually need large specimens whose preparation processes are time consuming and difficult especially for the preparation of green tape samples with uniform thickness. On the other hand, localized mechanical testing techniques which can provide the mechanical characteristics from small specimens

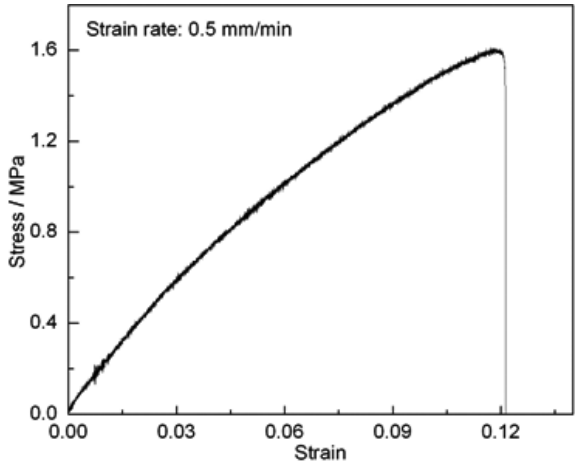

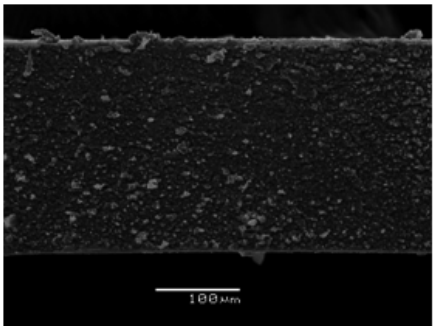

Fig. 2 Typical stress–strain curve and fracture surface of tensile specimens of green tape obtained from a sample parallel to casting direction.

Table 2 Tensile tests data of green tape at various strain rates.

Strain rate (mm min^{-1})	Parallel direction		Transverse direction	
	UTS (MPa)	Elongation (%)	UTS (MPa)	Elongation (%)
0.5	1.74 ± 0.08	10.65 ± 2.0	1.61 ± 0.2	12.5 ± 2.4
1	1.76 ± 0.07	13.6 ± 0.9	1.71 ± 0.06	13.4 ± 1.3
2.5	1.42 ± 0.2	10.95 ± 1.6	1.48 ± 0.3	10.4 ± 0.7
5	1.73 ± 0.09	10.95 ± 0.9	1.58 ± 0.001	15.1 ± 1.7

have generated much interest in recent years. SPT as one of the well-known examples of these miniature mechanical testing methods has been applied to a wide range of materials such as metals and alloys [34], composites [35, 36], and biomaterials [37]. This test is based on a blanking operation in which a flat cylindrical punch shears a disk specimen with the thickness usually in the range of a few hundred microns and the diameter more than 5 mm clamped between two die halves at constant speed [38, 39].

The shear punch load–displacement curves exhibited similar distinctive features such as transition and peak loads which show the repeatability of SPT data. The obtained curves which converted to shear strength *versus* normalized displacement using Eq. (1) can be divided along the strain axis into three regions of characteristic behavior, Figure 3. All curves displayed an initial linear region (Region I), used to measure elastic modulus, up to a transition load defined as shear yield stress (SYS). Region II as an extension region is from the onset of yield onwards until an increasing in shear stress and reaching a peak load characterized as ultimate shear stress (USS) in region III. Figure 4 represents the sheared surface of the ring-shaped portion and the central plug of the failed shear punch specimen. Shear-fractured surfaces are irregular with shear failure over most of the surfaces and some tensile failure at the margins. Surface of an interrupted test from region II in strain–stress curve is given in Figure 4c. From these micrographs, it can be concluded that shear punch samples experience an elastic deformation in region I which followed by shear failure for the most part of thickness with a almost constant load in region II and a final tensile pull out at region III.

Table 3 lists data obtained from load-displacement curves and calculated elastic modulus, SYS and USS. To the best of our knowledge, it is the first time any researcher has reported mechanical properties characterization of green tape by SPT and it was found to be a useful method for characterizing mechanical properties of green tapes.

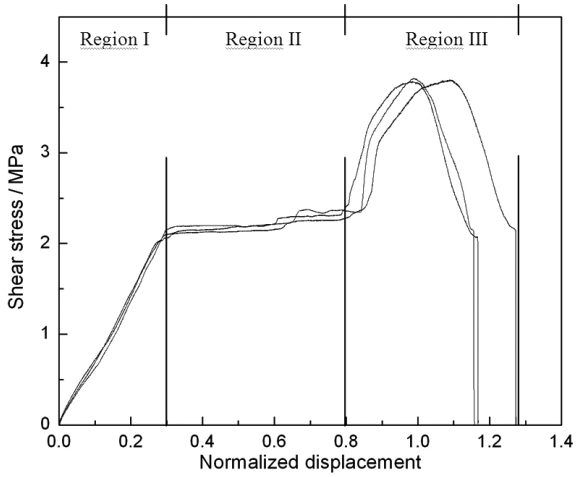

Fig. 3 Typical shear stress-normalized displacement curve of green tape obtained by SPT with crosshead speed of 0.25 mm min^{-1}.

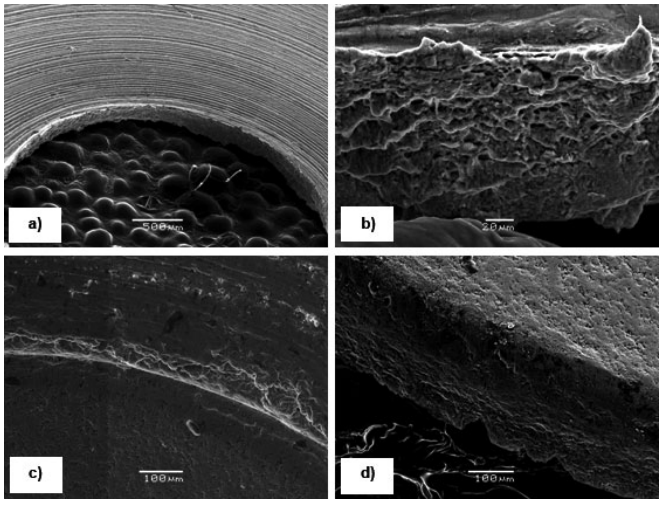

Fig. 4 Sheared surface created by the punch on (a and b) the ring-shaped portion (c) specimen of an interrupted test and (d) the central plug of the failed shear punch specimen.

Table 3 SPTs data of green tape at various strain rates.

Crosshead speed (mm min^{-1})	Transition load (N)	Peak load (N)	Elastic modulus (MPa)	SYS (MPa)	USS (MPa)
0.1	7.60 ± 0.94	13.69 ± 2.99	8.02 ± 2.81	2.08 ± 0.23	3.74 ± 0.72
0.25	6.93 ± 0.51	11.81 ± 0.51	7.23 ± 0.58	2.03 ± 0.17	3.55 ± 0.39
0.5	7.11 ± 0.64	11.09 ± 1.1	6.79 ± 0.89	2.07 ± 0.09	3.37 ± 0.36

3.2 *Mechanical Properties of Sintered Tapes*

Figure 5 shows the microstructures of sintered tapes at temperatures in the range of 1,300–1,500 °C. As it can be seen, the porosity decreased and grain size increased with increasing sintering temperature. There was no difference between the amount and shape of porosity in parallel and transverse cross section of sintered tapes. Figure 6 shows grain size distributions obtained at different sintering temperatures. Log-normal distribution is superimposed on experimental data, which provides a good fitting and mean normal grain growth occurred during sintering [40, 41]. Excessive grain growth is unavoidable during densification of 10GDC electrolyte by conventional sintering. However, to overcome this drawback of 10GDC, alternative processes such as adding sintering aids [42] or field assisted or flash sintering techniques has been reported [1, 4, 43]. Evaluating fracture surface of both transverse and casting direction of sintered tapes in high magnification shows that most of the pores left after organic burn off lying parallel with tape plan which are difficult to remove by sintering. As reported for fabrication of dense thin sheets [44–46], it seems hot pressing may help to achieve a dense layer in lower temperatures which would lead to a future study.

Table 4 gives computed flexural modulus and strength of tapes sintered at different temperatures which show that the mechanical properties increase with increasing sintering temperature and sintered tapes do not show significant anisotro-

ORIGINAL RESEARCH PAPER

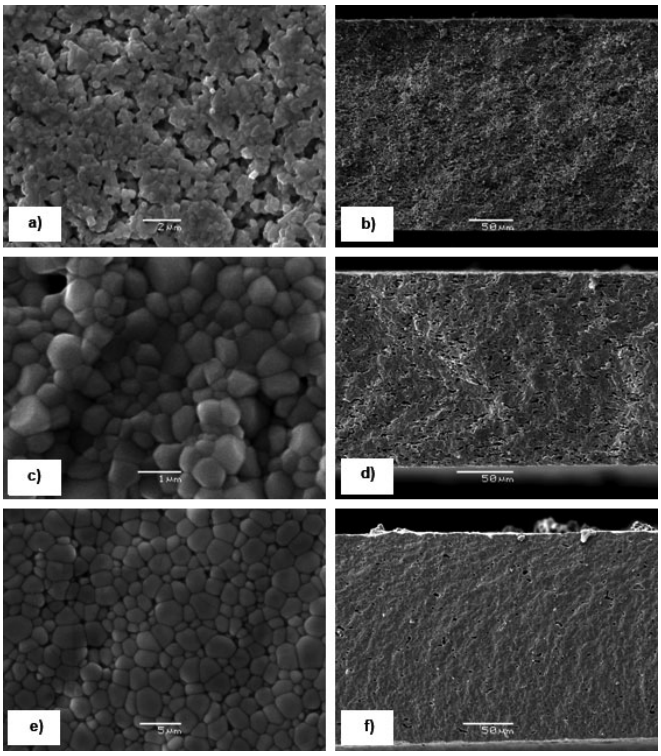

Fig. 5 SEM morphologies of tapes sintered at different temperatures for 2 h: (a) surface at 1,300 °C, (b) fracture surface at 1,300 °C, (c) surface at 1,400 °C, (d) fracture surface at 1,400 °C, (e) surface at 1,500 °C, and (f) fracture surface at 1,500 °C.

py related to casting direction. Increasing flexural strength with sintering temperatures is likely due to decreasing porosity left after burn out of organic additives. Reddy and Karan [47] reported flexural strength of 10GDC disks sintered at 1,300 °C, which is higher than the value obtained at this temperature but flexural modulus of the tape sintered at 1,500 °C is comparable with those obtained by nano-indentation for 10GDC [26].

Figure 7 shows the dependence of hardness with respect to the applied load for the sintered tapes at different temperatures. The hardness is gradually increased with the applied load, and with increasing sintering temperature the tapes exhibit higher hardness. Since the hardness is directly proportional to the sintered density [27], the samples having lower porosity showed higher hardness. Figure 8 shows the indentation marks observed on the samples. As it can be seen in Figure 8c and d, cracks have been observed near the indentation zones and intergranularly propagate through neighboring grains in the samples sintered at 1,500 °C, which can be used to calculate the fracture toughness. Many equations with some conditions and limitations have been proposed for measuring indentation fracture toughness as reviewed by Ponton and Rawlings [48].

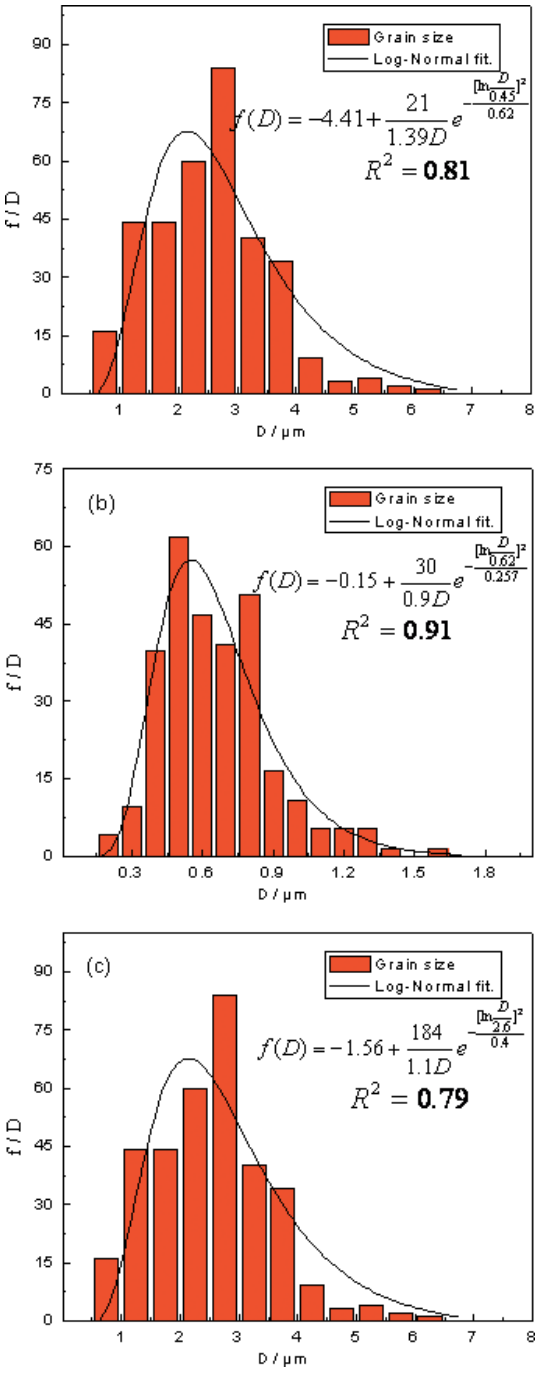

Fig. 6 Grain size distribution of tapes sintered at (a) 1,300, (b) 1,400, and (c) 1,500 °C 2 h^{-1}.

Table 4 Bending tests data and grain size of tapes sintered at different temperatures.

Sintering temperature (°C)	Grain size (μm)	Parallel direction		Transverse direction	
		Flexural strength (MPa)	Flexural modulus (GPa)	Flexural strength (MPa)	Flexural modulus (GPa)
1,300	0.41	80.2 ± 10.4	97.7 ± 21.2	86.2 ± 15.1	118.4 ± 16.6
1,400	0.61	113.6 ± 30.8	126.9 ± 37.6	103.9 ± 17.1	137.1 ± 10.8
1,500	2.25	127.4 ± 46.9	201.7 ± 77	116.9 ± 46.9	218.3 ± 50

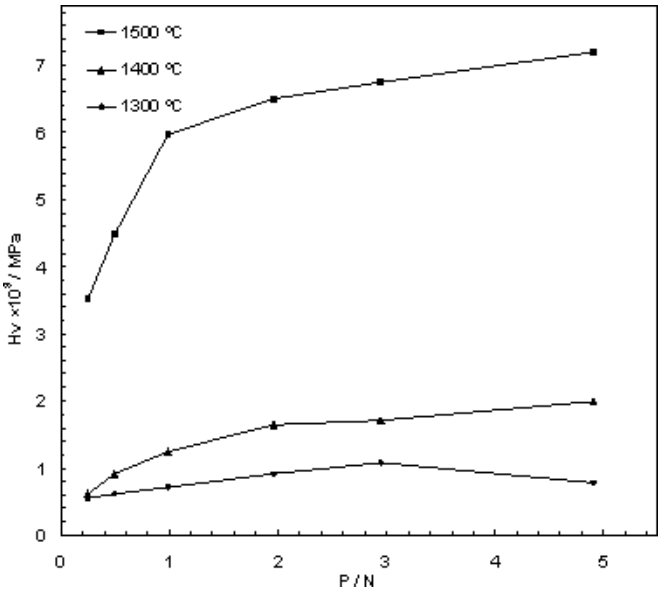

Fig. 7 Dependence of microhardness of tapes sintered at different temperatures as a function of load.

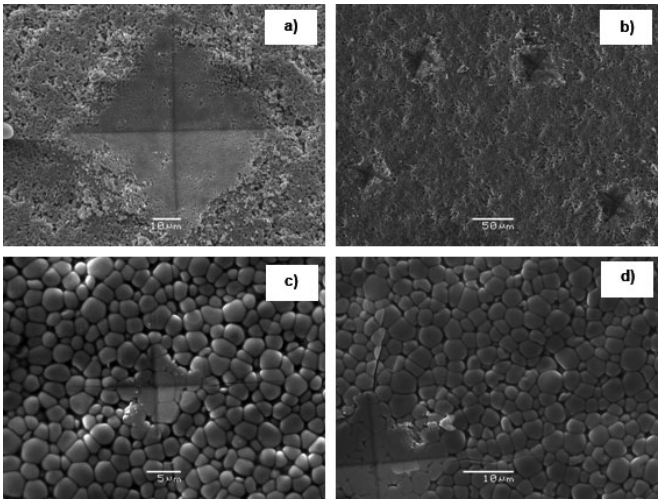

Fig. 8 Pyramid-shaped Vickers indentation marks on tape sintered at (a) 1,300, (b) 1,400 °C/2 h, (c and d) indentation imprint and emanated crack on the tapes sintered at 1,500 °C 2 h^{-1}.

Figure 9 shows the relation of half-diagonal of the indentation impression (a) and the crack length (l) obtained at different applied loads. Most of the data lie in the range of $0.4 \leq a/l \leq 1$, which was set by Niihara et al. for using Eq. (5). Calculated indentation fracture toughness versus applied loads showed almost equal hardness, is shown in Table 5. For comparison purpose, fracture toughness was also determined by Eq. (6), which used for indentation data reported for GDC. It appears that these results are comparable with those reported for 10GDC [27–29].

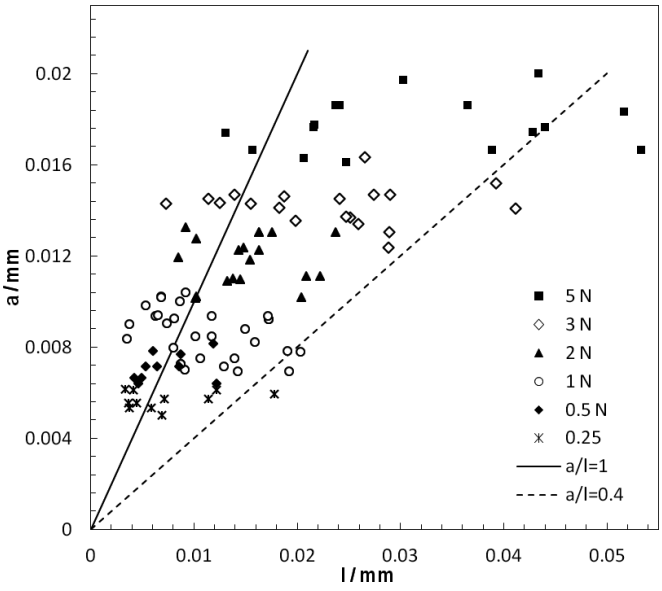

Fig. 9 Relation between the half-diagonal impression (a) and the indentation crack length (l) obtained at different applied loads.

Table 5 Hardness and fracture toughness measured with Eqs. (6) to (7) at different applied loads for tapes sintered at 1,500 °C 2 h^{-1}.

Applied load (N)	Hardness (GPa)	K_{IC} (MPa $m^{0.5}$) Niihara's eq.	K_{IC} (MPa $m^{0.5}$) Anistis's eq.
0.98	6.47 ± 1.68	1.37 ± 0.33	1.14 ± 0.43
1.96	6.67 ± 1.25	1.59 ± 0.25	1.31 ± 0.32
2.94	6.82 ± 0.83	1.64 ± 0.39	1.26 ± 0.50
4.90	7.29 ± 0.92	1.82 ± 0.40	1.35 ± 0.51

4 Conclusion

The GDC green tapes prepared by aqueous-based tape casting method were subjected to tensile and SPT for observing their mechanical strength. Maximum tensile strength of 1.76 MPa and shear strength of 3.74 MPa were obtained for as casted green tapes. SPT is a useful method to evaluate mechanical properties of green tapes. The tapes sintered at 1,300–1,500 °C were characterized for bending strength and microhardness. There was no significant anisotropy related to casting direction in both green and sintered tapes. Maximum flexural modulus of 218 GPa was obtained at traverse direction for 10GDC tapes sintered at 1,500 °C. Also, the microhardness of 7.3 GPa and fracture toughness of 1.82 MPa $m^{1/2}$ were observed at 4.9 N for 10GDC.

Acknowledgements

The authors acknowledge FONDECYT, Government of Chile (Project No.: 1100349) Direction of Investigation, University of Concepcion, Chile for the support to carry out this project.

References

[1] A. Akbari-Fakhrabadi, R. V. Mangalaraja, F. A. Sanhueza, R. E. Avila, S. Ananthakumar, S. H. Chan, *J. Power Sources* **2012**, *218*, 307.
[2] F. Tietz, A. Raj, D. Jungen Wand Stover, *Acta Mater.* **2001**, *49*, 803.
[3] B. Wang, R. J. Lewis, A. N. Cormack, *Acta Mater.* **2011**, *59*, 2035.
[4] X. Hao, Y. Liu, Z. Wang, J. Qiao, K. Sun, *J. Power Sources* **2012**, *210*, 86.
[5] R. A. Tsoga, A. Naoumidis, D. Stover, *Solid State Ionics* **2000**, *135*, 403.
[6] A. Moure, J. Tartaj, C. Moure, *J. Am. Ceram. Soc.* **2009**, *92*, 2197.
[7] C. Kleinlogel, L. J. Gauckler, *Solid State Ionics* **2000**, *135*, 567.
[8] P. L. Chen, I. W. Chen, *J. Am. Ceram. Soc.* **1993**, *76*, 1577.
[9] Q. L. Liu, S. H. Chan, C. J. Fu, G. Pasciak, *Electrochem. Commun.* **2009**, *11*, 871.
[10] Y. B. Go, A. J. Jacobson, *Chem. Mater.* **2007**, *19*, 4702.
[11] T. Mori, R. Buchanan, D. R. Ou, F. Ye, T. Kobayashi, J. D. Kim, J. Zou, J. Drennan, *J. Solid State Electrochem.* **2008**, *12*, 841.
[12] J. G. Cheng, S. W. Zha, J. Huang, X. Q. Liu, G. Y. Meng, *Mater. Chem. Phys.* **2003**, *78*, 791.
[13] F. Tietz, H. P. Buchkremer, D. Stover, *Solid State Ionics* **2002**, *152–153*, 373.
[14] T. Tian, D. Jiang, J. Zhang, Q. Lin, *Eur. Ceram. Soc.* **2007**, *27*, 2671.
[15] L. H. Luo, A. I. Y. Tok, F. Y. C. Boey, *Mater. Sci. Eng., A* **2006**, *429*, 266.
[16] C. Fu, S. H. Chan, Q. Liu, X. Ge, G. Pasciak, *Int. J. Hydrogen Energy* **2010**, *35*, 301.
[17] M. D. Snel, G. With, F. Snijkers, J. Luyten, A. Kodentsov, *J. Eur. Ceram. Soc.* **2007**, *27*, 27.
[18] D. J. Kim, I. S. Park, M. H. Lee, *Ceram. Int.* **2005**, *31*, 577.
[19] D. J. Shanefield, *Organic Additives and Ceramic Processing: With Applications in Powder Metallurgy, Ink and Paint*, Kluwer Academic Publishers, Boston, USA, **1995**.
[20] J. T. G. Overbeek, H. R. Kruyt, *Phenomenology of Lyophobic Systems*, Elsevier Publishing Comp., Amsterdam, The Netherlands, **1952**.
[21] J. V. Herle, T. Horita, T. Kawada, N. Sakai, H. Yokokawa, M. Dokiya, *Ceram. Int.* **1998**, *24*, 229.
[22] T. Xie, S. Jiang, M. Fan, *Ceram. Int.* **2009**, *35*, 2645.
[23] Z. Lv, T. Zhang, D. Jiang, J. Zhang, Q. Lin, *Ceram. Int.* **2009**, *35*, 1889.
[24] K. Y. Lim, D. K. Kim, U. Paik, S. H. Kim, *Mater. Res. Bull.* **2003**, *38*, 1021.
[25] M. Morales, J. J. Roa, X. G. Capdevila, M. Segarra, S. Piñol, *Acta Mater.* **2010**, *58*, 2504.
[26] R. V. Mangalaraja, S. Ananthakumar, U. Kasimayan, R. M. Jiménez, M. Lòpez, C. P. Camurri, *Mater. Sci. Eng., A* **2009**, *517*, 91.
[27] T. Zhang, Z. Zeng, H. Huang, P. Hing, J. Kilner, *Mater. Lett.* **2002**, *57*, 124.
[28] K. Sato, H. Yugami, T. Hashida, *J. Mater. Sci.* **2004**, *39*, 5765.
[29] A. Akbari-Fakhrabadi, R. E. Avila, H. E. Carrasco, S. Ananthakumar, R. V. Mangalaraja, *J. Alloys Compd.* **2012**, *541*, 1.
[30] K. Niihara, R. Morena, D. P. H. Hasselman, *J. Mater. Sci. Lett.* **1983**, *2*, 221.
[31] G. R. Anstis, P. Chantikul, B. R. Lawn, D. B. Marshall, *J. Am. Ceram. Soc.* **1981**, *64*, 539.
[32] R. Greenwood, E. Roncari, C. Galassi, *J. Eur. Ceram. Soc.* **1997**, *17*, 1393.
[33] J. R. Davis, *Tensile Testing*, Second Edition, ASM International **2004**.
[34] R. K. Guduru, K. A. Darling, R. Kishore, R. O. Scattergood, C. C. Koch, K. L. Murty, *Mater. Sci. Eng., A* **2005**, *395*, 307.
[35] C. A. Leon, R. A. L. Drew, *Mater. Lett.* **2002**, *56*, 812.
[36] P. Wanjara, R. A. L. Drew, S. Yue, *Mater. Sci. Technol.* **2006**, *22*, 61.
[37] S. M. Kurtz, C. W. Jewett, J. S. Bergstrom, J. R. Foulds, A. A. Edidin, *Biomaterials* **2002**, *23*, 1907.
[38] R. K. Guduru, A. V. Nagasekhar, R. O. Scattergood, C. C. Koch, K. L. Murty, *Metall. Mater. Trans., A* **2006**, *37*, 1477.
[39] R. Mahmudi, M. Sadeghi, *J. Mater. Eng. Perform.* **2013**, *22*, 433.
[40] P. Feltham, *Acta Metall.* **1957**, *5*, 97.
[41] B. Ralph, *Mater. Sci. Technol.* **1990**, *6*, 1139.
[42] C. J. Fu, Q. L. Liu, S. H. Chan, X. M. Ge, G. Pasciak, *Int. J. Hydrogen Energy* **2010**, *35*, 200.
[43] Y. Liu, X. Hao, Z. Wang, J. Wang, J. Qiao, Y. Yan, K. Sun, *J. Power Sources* **2012**, *215*, 296.
[44] Z. Lu, D. Jiang, J. Zhang, Q. Lin, *Ceram. Int.* **2011**, *37*, 293.
[45] P. M. Geffroy, T. Chartier, J. F. Silvain, *J. Eur. Ceram. Soc.* **2007**, *27*, 291.
[46] A. G. Adams, M. N. Rahaman, R. E. Dutton, *Mater. Sci. Eng., A* **2008**, *477*, 137.
[47] K. R. Reddy, K. Karan, *J. Electroceram.* **2005**, *15*, 45.
[48] B. C. Ponton, R. D. Rawlings, *Mater. Sci. Technol.* **1989**, *5*, 865.

